Formation of a Three-Dimensional Microstructure of Fe_3O_4−Poly(vinyl alcohol) Composite by Evaporating the Hydrosol under a Magnetic Field

R. Abu-Much,[†] U. Meridor,[‡] A. Frydman,[‡] and A. Gedanken*,[†]

Department of Chemistry and Kanbar Laboratory for Nanomaterials at the Bar-Ilan University Center for Advanced Materials and Nanotechnology, Bar-Ilan University, Ramat-Gan 52900, Israel, and Department of Physics, Bar-Ilan University, Ramat-Gan 52900, Israel

Received: December 7, 2005; In Final Form: January 17, 2006

In this paper, we report on the self-assembly formation of three-dimensional microstructures of Fe_3O_4 hydrosol. First, we perform new, facile, and direct fabrication of a stable hydrosol of Fe_3O_4 nanoparticles, based on the sonolysis of an aqueous solution of iron acetate in the presence of PVA-100 000. This is then followed by investigations of the formation of different microstructures obtained on drying a drop of the water suspension on a glass microscope substrate. The evaporation was carried out both without and in the presence of an external magnetic field.

Introduction

The synthesis of uniformly sized magnetic nanoparticles has been intensively pursued because of their broad applications, including magnetic storage media, ferrofluids, magnetic resonance imaging, and magnetically guided drug delivery.[1] Various methods have been reported on the synthesis of metal oxide nanoparticles, such as flame pyrolysis,[2] sol−gel reactions,[3,4] and chemical oxidation in micellar media or in polymer or mineral matrixes.[5]

However, one of the main challenges facing almost all of these novel techniques is the ability to transport and deliver well-dispersed nanoparticles with the desired composition, structure, and uniformity and the prevention of aggregation. A very important physical property of nanoparticles in general, and magnetic nanoparticles in particular, is their tendency to aggregate. Encounters between particles dispersed in liquid media occur frequently, and the stability of a dispersion is determined by the interaction between the particles during these encounters. The principal cause of aggregation is the van der Waals attractive long-range forces between the particles. To counteract these attractive interactions and promote stability, equally long-range repulsive forces are required.[6] They are obtained either by electrostatic repulsion between the particles or by coating the particles with organic long-chain molecules that act as surfactants.

Magnetic nanoparticles can be dispersed in carrier fluids through specific interactions between the particle surfaces and selected low-molecular-weight surfactants or polymeric surfactants. Such fluid dispersions of small magnetic particles are known as "ferrofluids".[7] Magnetic attractive forces combined with inherently large surface energies favor nanoparticle aggregation in magnetic dispersions.[8,9] Various methods have been reported for the preparation of stable dispersions of iron oxide in organic solvents (organosols), including hexane, decane, and the use of long-chain surfactants.[10,44]

Recently, we have described a sonochemical method for the preparation of a colloidal solution of iron oxide in Decalin by the use of oleic acid as a long-chain stabilizer.[11] However, for these organosols, the biological applications are greatly restricted because of their poor solubility in aqueous solutions. To realize their potential in biological applications, and to understand the environmental implications of these nanoparticles, it is important to develop a simple and generic method for the preparation of stable iron oxide hydrosols.

The synthesis of aqueous dispersions[45] of iron oxide is commonly performed by condensing divalent and trivalent iron salts in reactions with hydroxide bases (pH 9.5−10) and by the use of electrostatic stabilizers,[12] bilayer surfactants,[13−16] polymers as steric stabilizers,[17−21] and polymer templates.[22] However, in all these cases coating was accomplished ex situ, i.e., the nanoparticles were prepared first and then subjected to the surfactant solution under agitation. Recently we reported a sonochemical method for the synthesis of a stable hydrosol of Fe_3O_4 in a one-step process in the presence of sodium dodecyl sulfate (SDS) as a charged stabilizer, causing stability by electric double-layer interactions.[23] However, SDS cannot act as a protection layer for a long time against chemical instability with respect to oxidation under air. The preparation of well-ordered, multidimensional structures that cover large areas and possess useful properties, from the colloidal dispersion of nanoparticles, is becoming increasingly important due to their possible technical applications.[24,25] Over the last 10 years the self-assembly of nano- and microparticles deposited on substrates during the drying of colloidal solutions has been intensively investigated.[25−32] The important prerequisite for the self-assembly of colloidal-dispersed particles into well-ordered designs is the absence of agglomeration. The ability to study the behavior of magnetic particles of nanoscale dimensions is very important, as micromagnetic effects are a key issue for the future development of micromagnetic systems.

Many interesting articles can be found in the literature concerning the preparation of well-ordered, self-assembled arrays of noble metal particles.[26,28] Giersig and co-workers[47,48] investigated the effect of applied external magnetic fields during the drying of a Co colloidal solution, which resulted in the

* To whom correspondence should be addressed. E-mail: gedanken@mail.biu.ac.il.
[†] Department of Chemistry and Kanbar Laboratory for Nanomaterials.
[‡] Department of Physics.

10.1021/jp057123w CCC: $33.50
Published on Web 04/04/2006

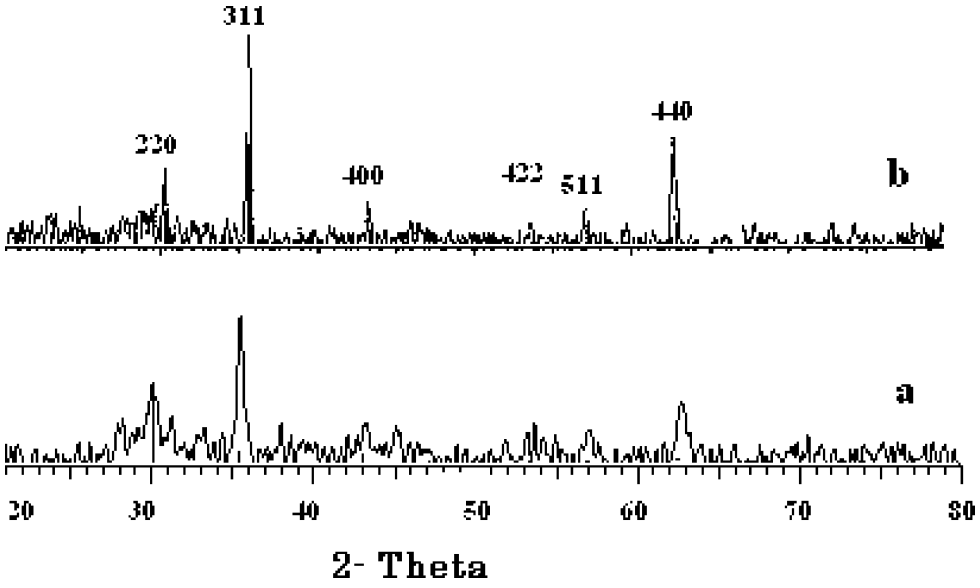

Figure 1. XRD pattern for (a) as-prepared Fe_3O_4 and (b) after heating as-prepared Fe_3O_4 to 700 °C.

creation of multidimensional structures. In theory, such micromagnetic structures offer a simple and cost-effective way to produce large-scale magnetic recording media.[33,46]

In this work, we explored the feasibility of synthesizing a stable aqueous dispersion of Fe_3O_4 nanoparticles by a sonochemical reaction.[37] Poly(vinyl alcohol) (PVA) is used both as a stabilizer and as a protecting layer against oxidation by the use of high-intensity ultrasound. The procedure that we report here, in comparison with common previous protocols reported in the literature, is a new, fast, and direct one-step process for the preparation of nonagglomerated Fe_3O_4−PVA composite nanoparticles dispersed in an aqueous solution. They resist oxidation for a long time due to the presence of long polymeric chains of the PVA on its surface.

After the preparation of the stable hydrosol of PVA-coated Fe_3O_4 nanoparticles, we investigated the self-assembly process of the arrangement of these nanoparticles when spread on a glass microscope substrate, and then we allowed the carrier solvent to evaporate. The effect of applying an external magnetic field during this process was also investigated.

Power ultrasound produces its effects via cavitation bubbles, which are generated during the rarefaction cycle of the sonic waves when the liquid structure is literally torn apart to form tiny voids that collapse during the compression cycle. It has been calculated that pressures of thousands of atmospheres and temperatures of thousands of degrees are generated upon the collapse of these bubbles. Chemical activation for sonochemical reactions is provided through the energy of the collapse of the cavitation bubbles. Volatile organometallic compounds decompose inside the cavitating bubble in a gas phase reaction to yield individual metal atoms. As these atoms agglomerate, they produce various highly porous nanostructures. Sonochemical reactions of nonvolatile compounds such as salts will occur in the interfacial region, which surrounds the collapsing bubble. Its width is calculated to be 200 nm, and the temperature reached after collapse 1900 K.[49]

2. Experimental Section

2.1. Chemicals. The precursors for this study were iron(II) acetate (Aldrich), poly(vinyl alcohol) (Fluka), sodium dodecyl sulfate (Merck), and a commercial Fe_3O_4 powder (Aldrich). All of these chemicals were used without further purification.

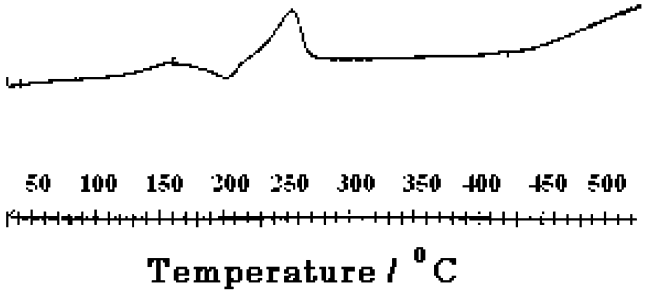

Figure 2. DSC trace of as-prepared Fe_3O_4.

2.2. Experimental Procedure. The experiment can be divided into two categories. In the first, we investigated and analyzed the formation of a powder consisting of Fe_3O_4 nanoparticles, and in the second, we studied the stabilization of the Fe_3O_4 nanoparticles by PVA and the formation of highly stable hydrosol. The synthesis of iron oxide powder was carried out as follows: a doubly distilled deoxygenated water solution of 0.1 M iron(II) acetate was subjected to a high-intensity ultrasonic horn (Ti-horn, 20 kHz) under 1.2 atm of Ar for 15 min. At the end of sonication a black precipitate of iron oxide nanoparticles was obtained. By the same procedure, a stable aqueous colloid solution of Fe_3O_4 nanoparticles was obtained by the addition of PVA (100 000) prior to the sonication. Different concentrations of the polymer in the range of 0.0002 M to 0.00004 M were used. The products were washed thoroughly with doubly distilled deoxygenated water in an inert glovebox (O_2 < 1 ppm) and dried under vacuum.

2.3. Fabrication of Micromagnetic Structures. After the preparation of stable colloidal solutions of Fe_3O_4 nanoparticles, we investigated the self-assembly formation of different microstructures by drying a drop of the water suspension on a glass microscope slide. The same process was applied under an external magnetic field parallel to the glass substrate. In this experiment, the solvent slowly evaporated and the magnetic field (∼0.01−0.3 T) was applied until the evaporation was completed. At the end of the evaporation, we could observe the formation of large areas of dendrite domain microstructures of Fe_3O_4 nanoparticles. However, by applying a higher magnetic field strength (∼0.5 T), regular linear arrays were formed. To check the role of the stabilizer in the formation of the dendrites, we changed the surfactant to SDS, and as a result, a colloidal

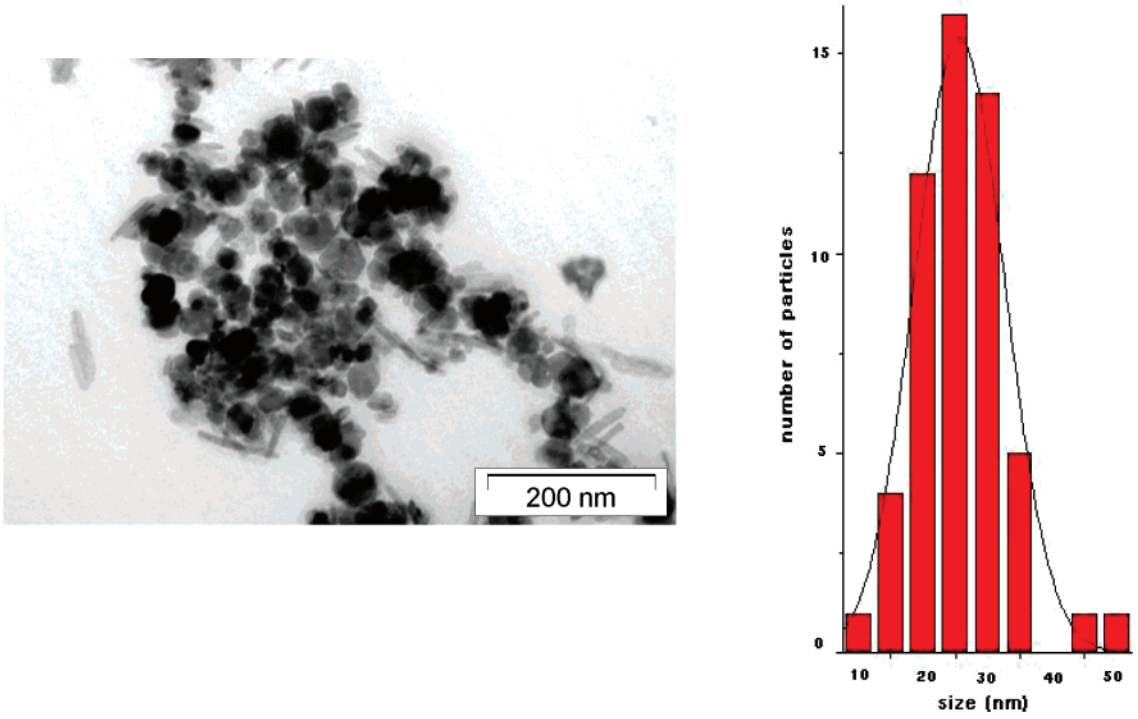

Figure 3. TEM micrographs of sonochemically prepared Fe_3O_4.

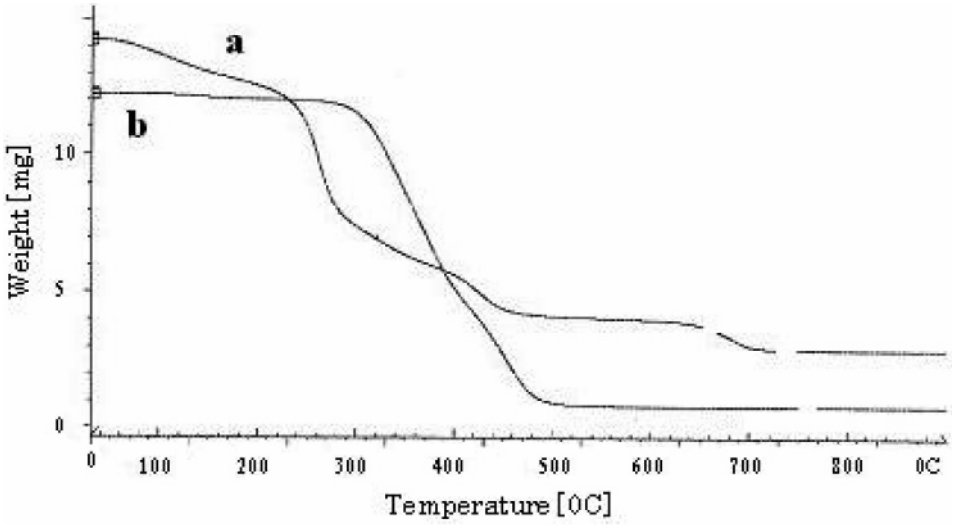

Figure 4. TGA curves of (a) Fe_3O_4−PVA composites and (b) pristine PVA.

aqueous solution, stable for a few hours, was obtained. Applying the same evaporation process by drying a drop of the SDS solution on a glass microscope substrate both with and without an external magnetic field led to different microstructures.

2.4. Analysis and Characterization. The characterization of the aqueous colloidal suspension was conducted by energy-dispersive X-ray spectroscopy (EDX) and transmission electron microscopy (TEM). A Scion image software program was used to measure the distribution of particle size by measuring more than 100 particles from the TEM image. In the thermal analysis (thermogravimetric analysis [TGA] and differential scanning calorimetry [DSC]) experiments, the sample was heated to 700 °C at a rate of 10 °C per minute, under a nitrogen atmosphere. The TGA and DSC measurements were conducted by a Mettler Toledo TGA/SDTA851 and a Mettler Toledo DSC 25, respectively. The X-ray diffraction (XRD) measurement was carried out using a Model-2028 (Rigaku) diffractometer. The Raman spectrum was recorded on a Raman instrument, Jobin Yvon Horba. The ζ-potential measurements were employed to investigate the stabilization mechanism of PVA, using a Zetasizer $3000H_{SA}$ Malvern instrument. Magnetization was measured using a Quantum Design MPMS SQUID magnetometer; External magnetic field was recorded by Horizon Electronics, Alpha Scientific Berkeley No.7500. Magnetic force microscopy (MFM) and atomic force microscopy (AFM) were carried out using a DI-Digital Instruments Nanoscope Dimension 3100 controller. Optical Images were recorded by the Olympus BX51 ColorView Soft Imaging System.

3. Results and Discussion

The sonochemical process presented here provides a rapid one-step synthesis of a stable aqueous solution of Fe_3O_4 nanoparticles. The colloidal solution that uses the PVA as a stabilizing agent was found to be stable for at least one year. PVA acts both as a stabilizer and as a protecting layer against

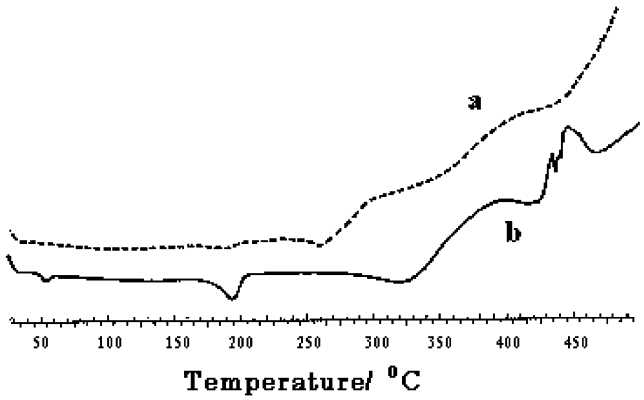

Figure 5. DSC curves obtained from (a) Fe_3O_4−PVA composites and (b) pristine PVA.

oxidation for long-time exposure to ambient conditions. The process of the preparation of a powder of Fe_3O_4 was reported elsewhere,[37] and therefore only part of the characterization process is repeated herein.

3.1. Characterization of an Fe_3O_4 Nanoparticle Powder Resulting from the Sonochemical Reaction. The first step in our work was to analyze the nanometer-sized Fe_3O_4 particles formed without the addition of PVA. The XRD diffraction patterns of the as-prepared product, as well as the product after annealing at 700 °C for 3 h, are presented in parts a and b of Figure 1, respectively. The as-prepared sample showed low-intensity diffraction peaks, whereas the heated sample shows sharp crystalline peaks. This indicates that the majority of the as-prepared sample is in the crystalline form and was confirmed by the exothermic peak in the DSC trace (Figure 2). It can be clearly seen that the diffraction pattern matches that of Fe_3O_4.[34] The mean crystalline size calculated from the width of the XRD peaks of the as-prepared powder, using Scherrer's equation,[50] is 21.3 nm.

Magnetite differs from most other iron oxides in that it contains both divalent and trivalent iron. Its formula is written as Y [XY]O_4 where X = Fe^{II}, Y = Fe^{III}, and the brackets denote octahedral sites.[43] To confirm the existence of both ions, a well-known spot test is used.[38] This method is based on the fact that Fe^{II} salts in acidic solutions react with α,α-phenanthroline to give a soluble, dark red complex. Fe^{III} salts do not react under these conditions. This spot test was performed for the as-prepared dried black powder, commercial Fe_3O_4, and commercial Fe_2O_3. The tests revealed a dark red color for the dried black powder, as well as for commercial Fe_3O_4. A colorless solution was observed for commercial Fe_2O_3. This spot test

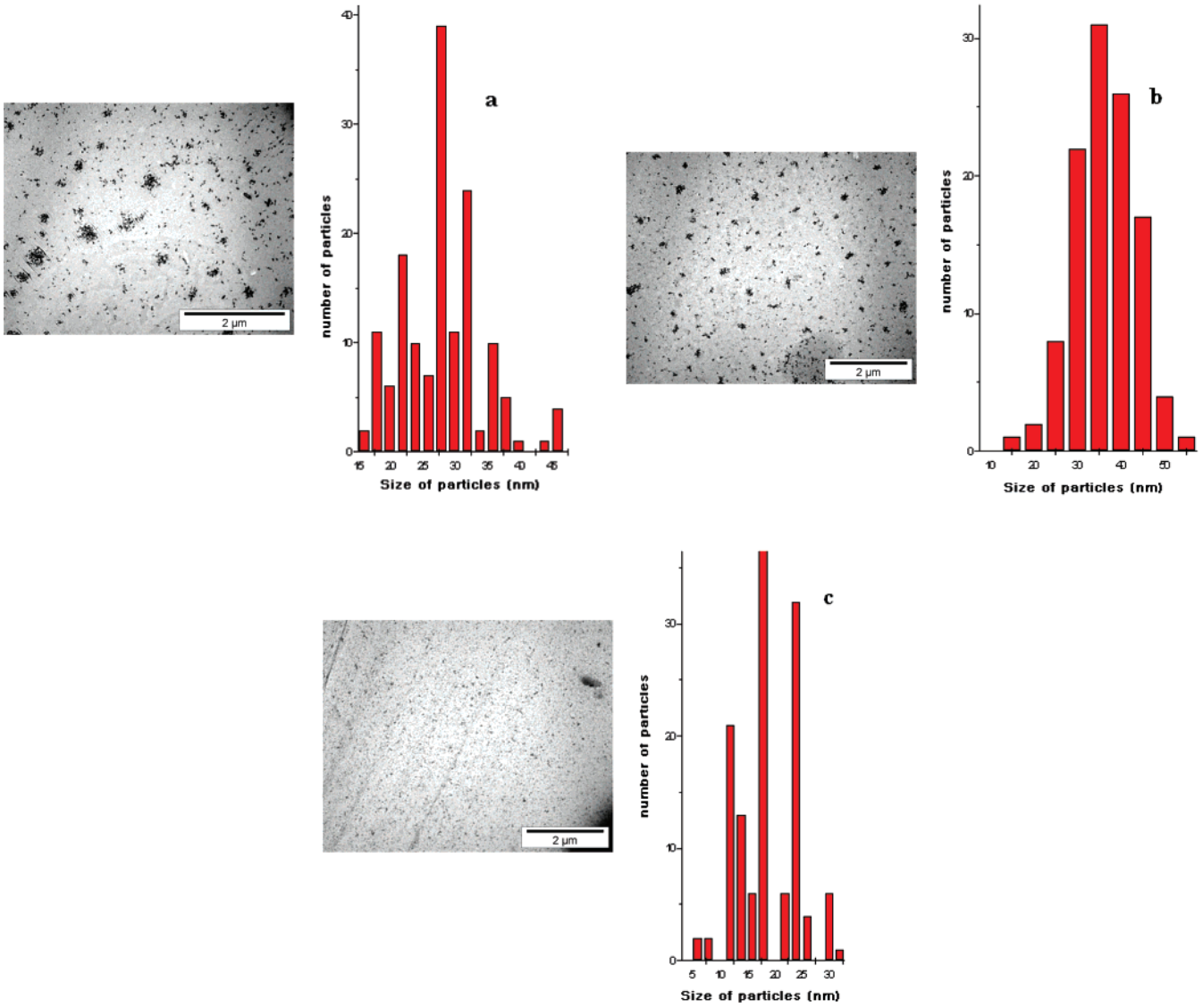

Figure 6. TEM of Fe_3O_4−PVA with molar ratio of (a) 1/500, (b) 1/1000, and (c) 1/1500.

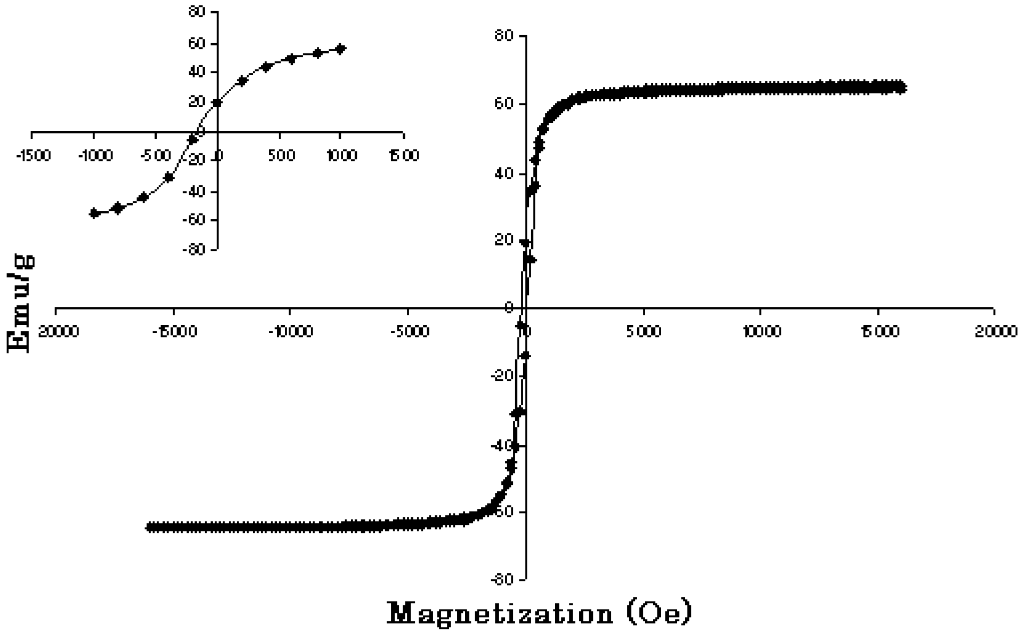

Figure 7. Magnetization loop of the iron oxide nanoparticles powder measured at room temperature. Inset: A magnified picture of the origin region.

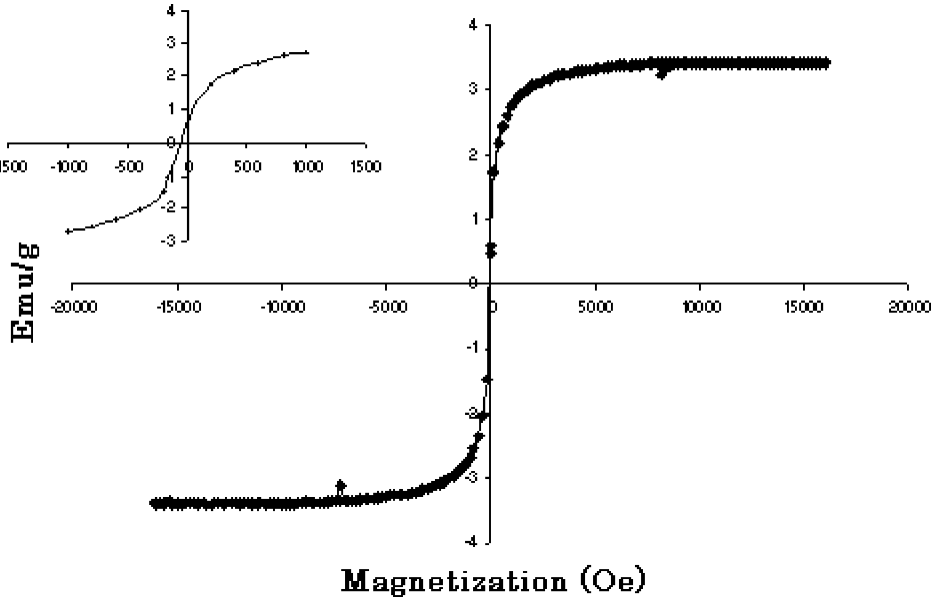

Figure 8. Magnetization loop of the iron oxide−PVA nanoparticles measured at room temperature. Inset: A magnified picture of the origin region. The Fe_3O_4:PVA molar ratio was 1500:1.

provides more support for the identification of the black powder as Fe_3O_4. We have repeated the spot test for the argon-heated sample and detected the same color as observed for the as-prepared product. This check ascertains that the heated sample is also Fe_3O_4. The mass profile obtained by the thermogravimetric plot for the as-prepared sample shows a weight loss of about 20% at a temperature up to 110 °C, which can be attributed to the loss of water and any adsorbed species.

The DSC trace (Figure 2) reveals an initial small endothermic peak that can be related to the loss of water and which is further supported by the corresponding weight loss in the TGA curve. Furthermore, a distinct exothermic peak at around 240 °C is detected and assigned to an amorphous-to-crystalline transition. This peak is not observed in a second heating cycle.

Figure 3 shows the TEM photograph of the as-obtained Fe_3O_4 powder. It also shows the aggregated form of the nanometer-sized particles. A histogram representing the average size of the aggregated nanoparticles, using Scion Image Software, revealed that the agglomerates consist of small nanoparticles in the form of large aggregates.

3.2. Stabilization by PVA-100 000. In the process presented here, we perform the facile and direct fabrication of a stable hydrosol by introducing the PVA into the sonication cell so that as soon as the Fe_3O_4 particles are formed they are almost simultaneously coated with PVA-100 000. In the following section we will describe the way in which the stable solution is analyzed, and we will investigate the unique structures of these nanoparticles under different conditions.

The thermogravimetric plot of the Fe_3O_4−PVA composites is depicted in Figure 4a; the initial weight loss of about 15% at temperatures up to 110 °C is attributed to the loss of water and any physically adsorbed species. A further weight loss detected between 220 and 270 °C is related to the degradation and loss of PVA-100 000 in the composite. This assignment is based on

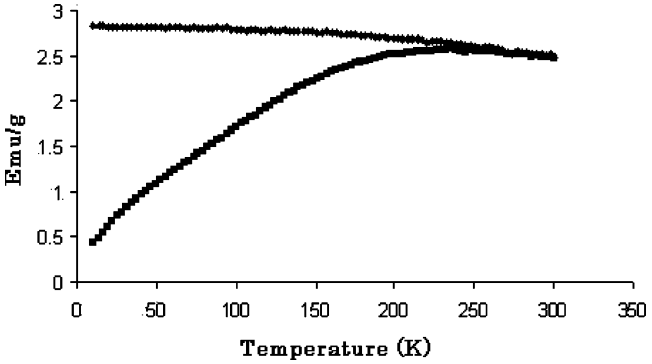

Figure 9. Temperature-dependent magnetization of Fe_3O_4−PVA composite in zero field cooled and field cooled conditions. The measurements were taken at a field of 100 Oe. The Fe_3O_4:PVA molar ratio was 1500:1.

the TGA of the pristine PVA illustrated in Figure 4b. The decomposition of the pristine polymer occurs at higher temperatures than the composite. The magnetite nanoparticles weaken the interchain interactions and lead to polymer decomposition at lower temperatures. Our explanation for this dependence is as follows: the perturbation that the particles introduce affect the three-dimensional (3-D) structure of the polymer. This perturbation weakens the van der Waals interactions between the stability of the polymer, which is reflected by the lowering of the decomposition temperature.[51,52]

The DSC plot for the as-prepared iron oxide nanoparticles stabilized by PVA-100 000 is shown in Figure 5a. The observation of an endothermic peak at ∼190 °C is related to the PVA, as shown in Figure 5b. An exothermic transition is detected around 300 °C and assigned to the crystallization of the Fe_3O_4 nanoparticles. This peak does not show up in the second heating cycle. The decomposition of PVA can be assigned to the endothermic peak at 260 °C.[42] This assignment is supported by the TGA measurements, which reveal a weight loss in the temperature range of 240−280 °C. It is also possible that the decomposition occurs at higher temperatures, overlapping the crystallization of the magnetite.

A most important physical property of colloidal dispersions is the tendency of the particles to aggregate. Encounters between particles dispersed in liquid media occur frequently, and the stability of the dispersion is determined by the interaction between the particles during this encounter.

To promote a stable dispersion, long-range repulsive forces are required in order to keep each particle discrete and prevent it from amassing as larger and faster settling agglomerates. Steric hindrance is one of the major surface forces playing an important role in stabilizing suspensions. This is accomplished by the coordination of sterically demanding molecules or polymers that act as protective shields on the oxide surface.[6] In our case, we demonstrate that uncharged poly(vinyl alcohol) (PVA-100 000) is a good surface-active agent. An aqueous solution of PVA has a strong adhesion to a hydrophilic substance, and the adhesion tends to increase with the degree of hydrolysis and polymerization. According to the literature, PVA is known to adsorb on oxide surfaces.[36] The interaction with the surface can result from hydrogen bonding between the polar groups of the polymer and the surface of the oxide. A ζ-potential measurement is considered a key parameter for providing an insight into the charge of the iron oxide nanoparticles. The ζ-potential measurements were carried out for the colloidal solution in a pH range of 6−7. The measurement yielded a ζ-potential of 3.8 mV. This very low positive value is not enough to achieve electrostatic repulsion, and it indicates that the stabilization can be related

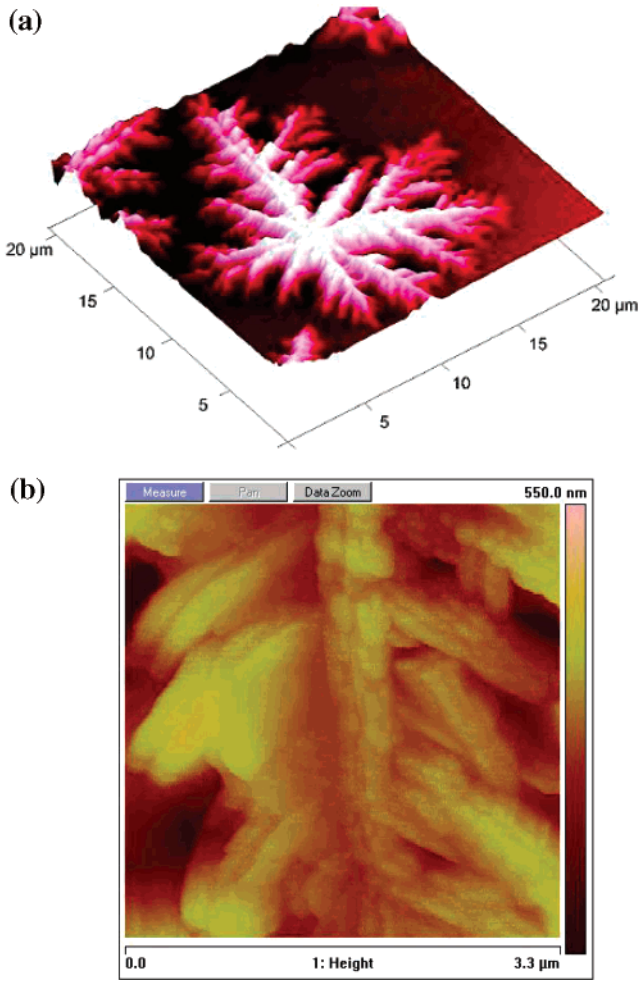

Figure 10. (a) AFM image of dendrite structure, obtained after the evaporation process. (b) AFM image of 2-D tree border of a dendrite structure.

to the steric hindrance mechanism caused by the coating of the PVA long chains, which lead to the creation of a protecting layer around each particle. The stable dispersions of Fe_3O_4 nanoparticles were prepared with a different molar ratio of a PVA/precursor by varying the concentration of PVA in the range of 0.0002 M to 0.00004 M. The results obtained show that the molar ratio of 1/1500 is considered as a critical ratio. Below this ratio, no stable dispersion is obtained. Parts a, b, and c of Figure 6 present TEM micrographs obtained by a PVA/iron acetate molar ratio of 1/500, 1/1000, and 1/1500, respectively. The images illustrate clearly that the nanoparticles are highly dispersed. The figures verify that only a very small number of the particles are left aggregated. The stability of the suspensions is achieved because of the strong repulsion forces related to the polymer layer on the particle's surface.

Histograms of size distribution by means of Scion Image Software were obtained by measuring more than 100 particles from each TEM image. We found particles whose average size was 27.8, 36.3, and 18.5 nm, obtained by molar ratio of PVA/precursor of 1/500, 1/1000, and 1/1500, respectively.

3.3. Magnetic Results. The magnetization of ferromagnetic Fe_3O_4 bulk material is very sensitive to the microstructure of the sample. Superparamagnetism occurs when the particle is small enough that thermal fluctuations (these are of order kT) can overcome the magnetic *anisotropy* (this is of the order of KV, where K is the anisotropy constant and V is the particle volume). Once this happens the magnetization of the particle

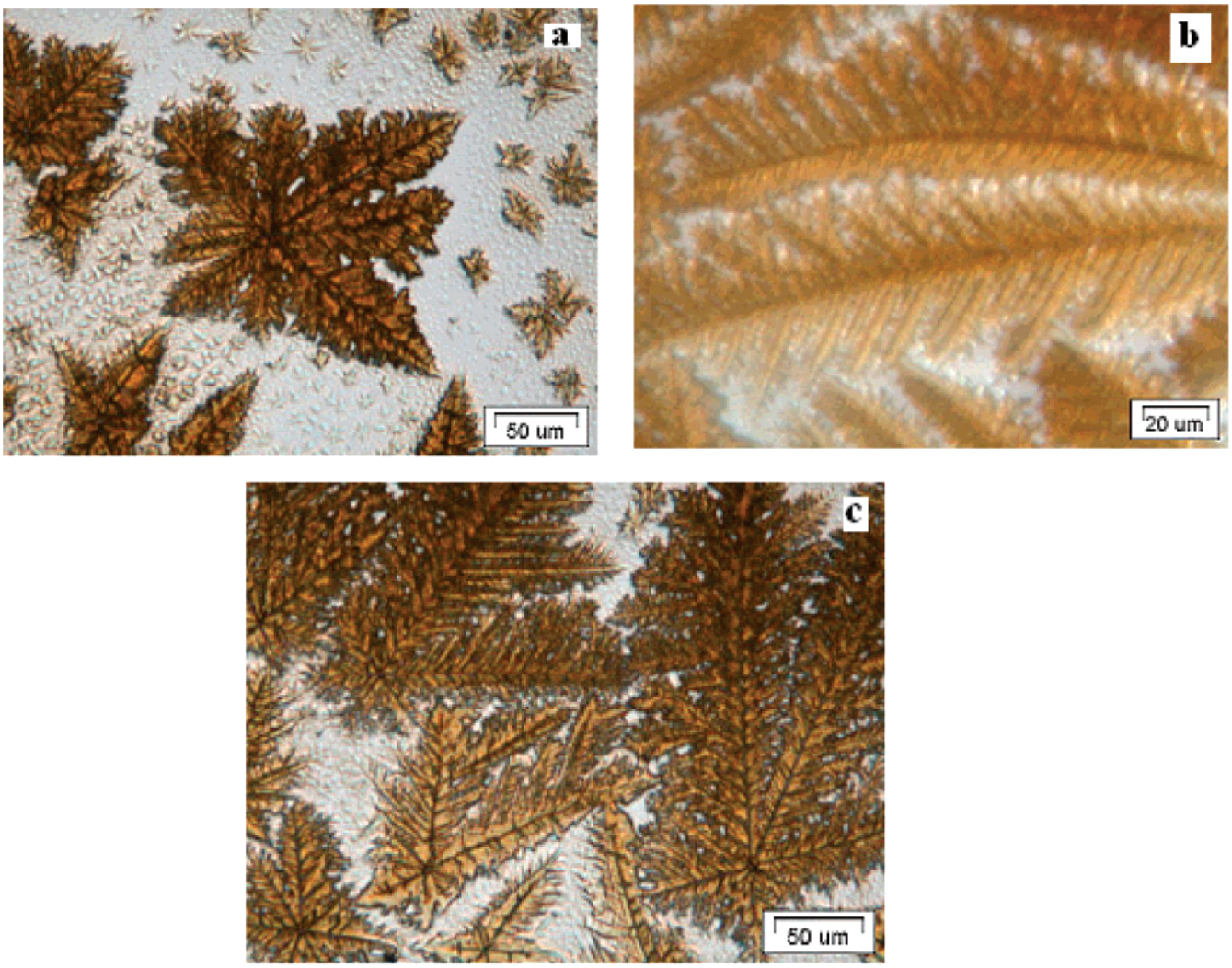

Figure 11. (a) Optical microscope image of dendrite structures of different sizes. (b) Optical microscope image of a frond branch of dendrite structure. (c) Optical microscope image of huge dendrite structures.

is no longer fixed along a certain direction (determined by the easy magnetic direction of the lattice) but precesses at random, in which each particle acts as a big "spin" with suppressed exchange interaction between the particles. The lack of hysteresis is one of the criteria required for the identification of the product as superparamagnetic. We performed a set of magnetization measurements in order to try to characterize the size distribution of the particles.

The room temperature magnetization loop of the as-prepared Fe_3O_4 powder and of Fe_3O_4−PVA nanocomposites are presented in Figures 7 and 8, respectively. It is seen that the loops show very small hysteresis with coersive fields of 150 and 80 Oe and remnant magnetization of 20 and 0.7 emu/g for the pristine Fe_3O_4 and the Fe_3O_4−PVA, respectively, indicating that the average size of the particles reduces as PVA is introduced.

Figure 9 depicts the magnetization versus temperature under zero field cooling, and field cooling conditions for the Fe_3O_4−PVA system. The results on the Fe_3O_4−PVA samples are consistent with superparamagnetic colloids having a blocking temperature of about 200 K.

3.4. Fabrication of Micromagnetic 3-D Dendrite Structures. The stable hydrosol of Fe_3O_4−PVA nanocomposites was investigated for its self-assembly organization on flat surfaces. This was done by the evaporation of a drop of the ferrofluid on a glass microscope substrate. The evaporation was carried out with and without a magnetic field applied parallel to the substrate plane. The effect of the strength of the applied magnetic field was also investigated. The fabrication of the magnetic microstructures was followed by optical microscopy, AFM, and MFM measurements. The evaporation process without an external magnetic field created sharp dendrite structures, as illustrated in Figure 10a,b.

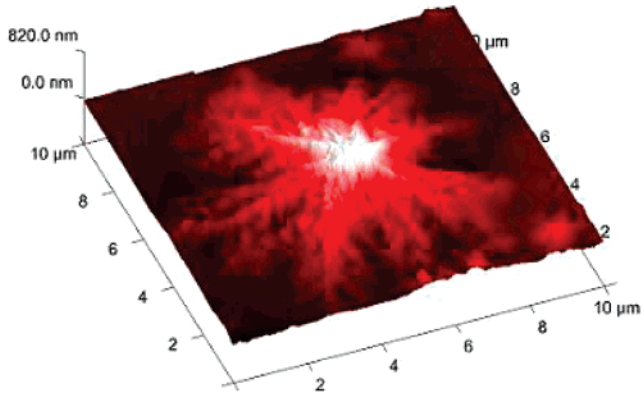

Figure 12. MFM images obtained by the evaporation process under a magnetic field of ~<0.01 T.

The formation of clear dendrite structures during the evaporation process did not reveal a unified dendrite size, as can be seen from the optical microscopy images shown in Figure 11.

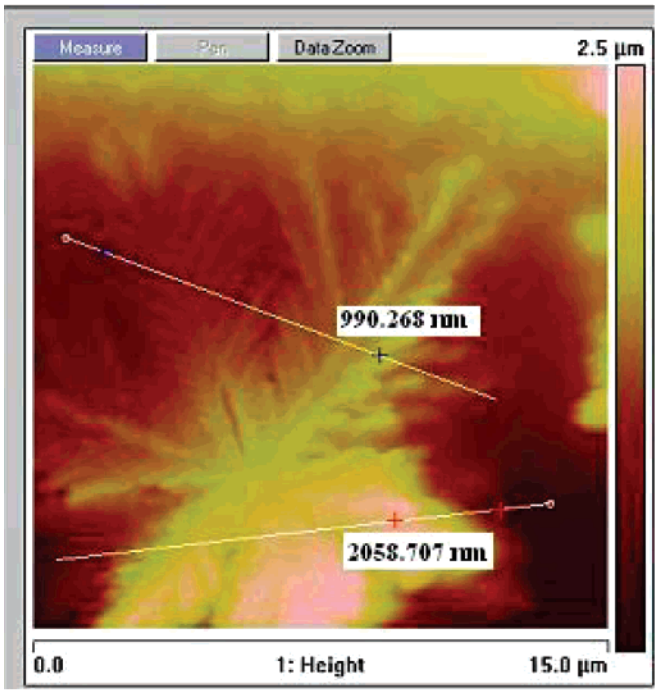

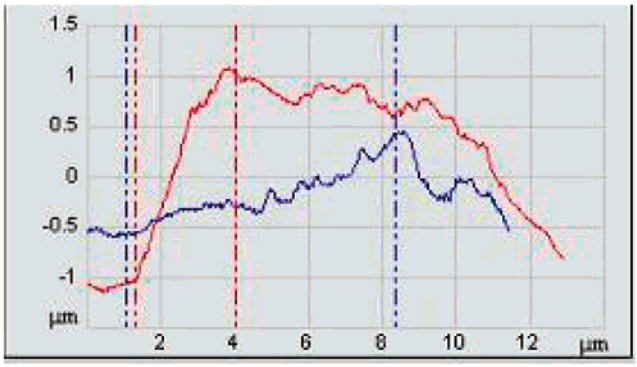

Figure 13. An example of the calculation of height of a dendrite formed under a low magnetic field.

The size of the dendritic structure varied from ~10 to ~150 μm. Analysis of the height of these dendrite structures along a *Z*-axis indicates that it is in the range of 250−400 nm.

We could investigate the effect of applying magnetic field during the evaporation process on the specific mode of agglomeration of the nanocomposites and the formation of dendrite structures. Figure 12 depicts a 3-D AFM image obtained under the application of a low magnetic field (~ 0.01 T). It demonstrates the formation of dendrite structures with highly orientated dendrites along the *Z*-axis, as compared with those formed in the absence of a magnetic field. Tree-like structures were observed as the major structured product upon the application of an external magnetic field.

Figure 13 presents a calculation of the height of the dendrite structure along the Z-direction obtained under a low magnetic field.

As can be seen, the analyses were carried out at different regions in the dendrite structure. The calculations revealed a significant distinction of the height along the *Z*-axis, as compared with those obtained in the absence of a magnetic field. It varied from ~1 μm at the end of the dendrite to ~2 μm in the middle.

We have gradually increased the intensity of the magnetic field and followed the structural changes of the crystal growth of the Fe_3O_4−PVA composite. We could follow the structural change from the tree-like dendritic structure at a low magnetic field to linear dense layers at the highest magnetic field. At an intermediate magnetic field, we could follow the reduction in size and the amount of the dendrites, accompanied by the formation of the straight line. These images reveal that the growth of nanocomposites is affected by a magnetic field, and at stronger fields lead to organization along the field direction. These results are depicted in Figures 14 and 15 obtained by optical microscopy.

We can clearly see that the strongest magnetic field (0.5 T) leads to the development of regular microstructural arrays of particles. It was difficult to obtain obvious images by MFM for these regular arrays because of the large height regions produced. To check the effect of the PVA chain on the behavior of the nanoparticles during the evaporation process, we tried to

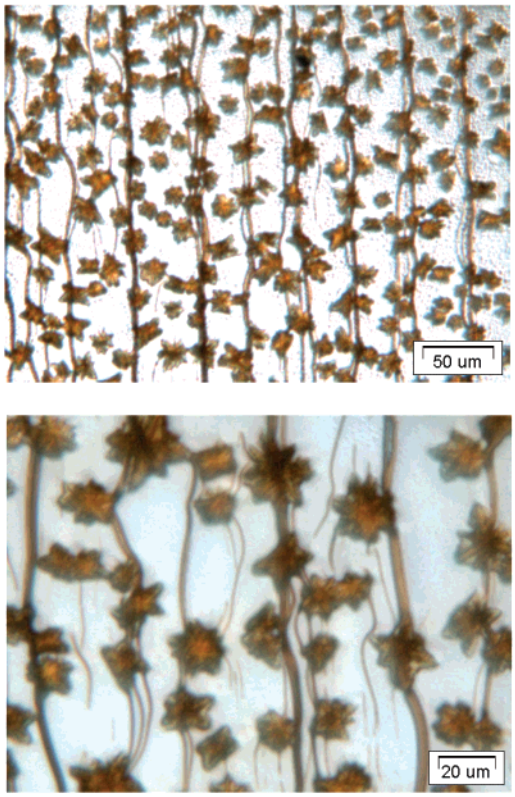

Figure 14. Optical microscope images obtained by the evaporation process under a magnetic field of 0.3 T.

change the surfactant to SDS. Although the stability of this colloidal solution lasts for just a few hours, it was long enough to investigate the evaporation process under an applied field or in its absence. The results obtained revealed different microstructures from those of the PVA−Fe_3O_4 composite. The evaporation process conducted without an external magnetic field led to the formation of spherical agglomerated structures, while under a magnetic field of 0.3 T, the particles were organized similarly to the magnetite−PVA composite, namely,

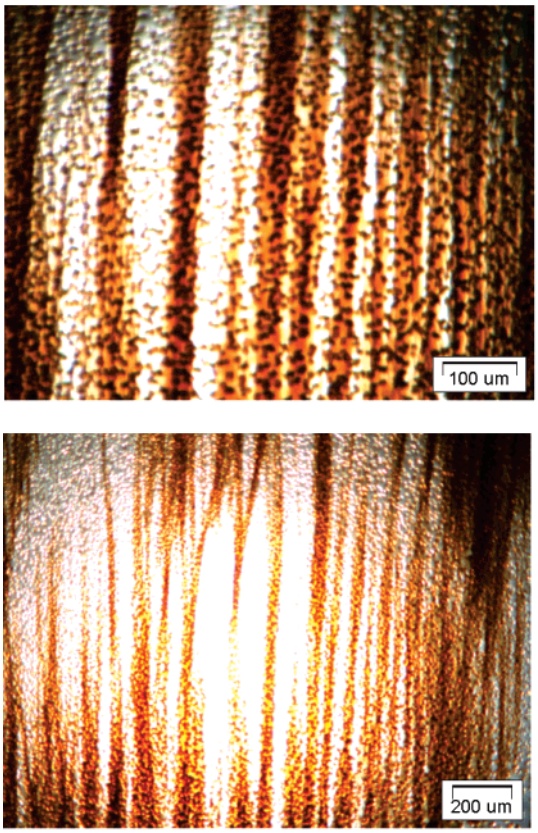

Figure 15. Optical microscope images obtained by the evaporation process under a magnetic field of 0.5 T.

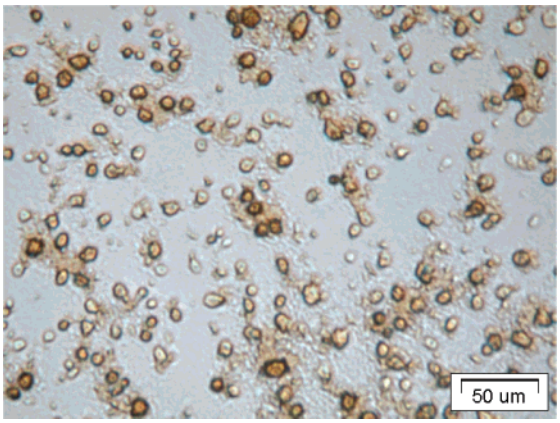

Figure 16. Optical microscope image obtained by the evaporation process in the absence of field and a histogram representing the aggregate size.

in the form of regular lines. In Figures 16 and 17 we present the images of the Fe_3O_4−SDS structures formed in the solvent evaporation with and without a magnetic field.

3.4.1. Discussion. An understanding of the origin of snowflake shapes and other such nonequilibrium growth patterns has fascinated physicists. Recent experimental and theoretical developments have revealed unexpected similarities among ostensibly different physical systems. Different theoretical approaches were offered toward the elucidation of these issues. Theoretical treatments of the mechanisms leading to these extremely complex patterns are in agreement that free dendrites are always linearly stable.[39] They generally form smooth needle crystals, but rather generate a continuous stream of side branches. The principal growth characteristics are the approximate constant velocity and paraboloidal shape of the tip,

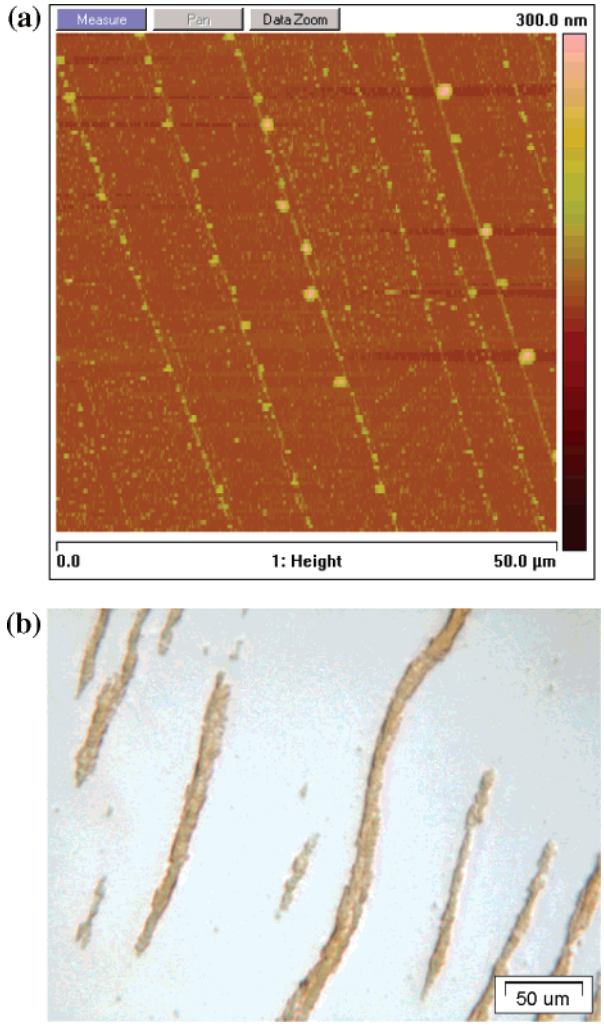

Figure 17. Image obtained by evaporation under field: (a) MFM image, (b) optical microscope image.

and the evenly spaced side branches that begin to produce their own secondary side branches as they grow. Pieters and Langer[40] were the first to suggest that side branches might be understood as a response of the system to noise. Numerical methods have been used to investigate the effects of noise, and they have revealed that the steady-state response of the system to noise is a plane wave. So if we drive the system with the source of the noise, the solution at large distances will be a plane wave of a unique wave vector, which has the strongest spatial amplification. Numerical treatments revealed that there is a frequency of noise (Ω^*) for which the spatial amplification is a maximum. Thus, noise with frequencies near this particular frequency will be selectively amplified as one moves further a way from the tip. We expect that once the noise amplitude increases beyond a small value, nonlinear effects will stabilize the perturbation and side branches will be observed.

Up to now, we have discussed the principal growth characteristics of the dendrites. We also have to consider that the final structure of the interface system can be controlled by diffusion. Diffusion-limited aggregation (DLA), introduced by Witten and Sander,[41] exhibits a satisfying model to study aggregation processes. It represents noisy growth limited by diffusion that consists of a single cluster, which grows by the attachment of random walkers to its boundary. We believe that a Brownian motion of colloidal particles plays an important role during colloidal aggregation, similar to DLA. DLA has maximal

noise: the fluctuations in the velocity are of the same magnitude as the velocity itself.

We believe that the external magnetic field causes the existence of preferential directions of growth. It exhibits an external effect inducing a means of anisotropy during crystal growth. At a high magnetic field, we could clearly observe linear regular arrays made of dendrite structures, which is an indication of preferential growth process.

In our system, we assume the existence of competition between diffusion forces caused by the Brownian motion of the stabilized particles and their magnetic interactions. A shell of long-chain polymer that surrounds each particle is a key factor in controlling the microstructure, and it causes the diffusion parameters to change toward magnetic interactions. As a result, particles have more freedom of motion and are driven by diffusion. By applying a high external magnetic field, particles "prefer" to aggregate along the direction of the field rather than form random branches. The pattern of dendrite structure changes into a chainlike structure along the direction of the external magnetic field. This process is attributed to the change in interaction between the particles that control the system. Without a magnetic field, diffusion parameters are dominant and particles undergo a pure Brownian motion and form random branches. We believe that an external magnetic field induces competition between diffusion and magnetic interactions. When the magnetic field is very low, the system is basically still affected by diffusion factors. On the other hand, under a high magnetic field, the controlling interaction changes into magnetic interactions, and as a consequence, particles prefer to aggregate along the direction of the external magnetic field. Diffusion forces still exist as a perturbation, but are not dominant, and result in the observation of unclear dendrites along the regular chains.

Replacing long-chain PVA by SDS resulted in the disappearance of dendrite fractal structures. This is due to the extensive magnetic interactions between the particles. We believe that short chains (SDS) surrounding the surface of each particle provide a key for larger interparticle interactions, and the aggregation is a function of a combination between the Brownian motion and interparticle forces. As a consequence, noisy growth limited by diffusion is restricted, exhibiting anisotropic growth along the direction of the external magnetic field.

References and Notes

(1) (a) Sun, S.; Murray, C. B.; Weller, D.; Folks, L.; Moser, A. *Science* **2000**, *287*, 1989. (b) Awschalom, D.; DiVicenzo, D. P. *Phys. Today* **1995**, *4*, 43. (c) Leslie-Pelecky, D. L.; Rieke, R. D. *Chem. Mater.* **1996**, *8*, 1770. (d) Raj, K.; Moskowitz, R. *J. Magn. Magn. Mater.* **1990**, *85*, 233. (e) Speliotis, D. E. *J. Magn. Magn. Mater.* **1999**, *193*, 29. (f) Raj, K.; Mostowitz, B.; Casciari, R. *J. Magn. Magn. Mater.* **1995**, *149*, 174. (g) Oswald, P.; Clement, O.; Chambon, C.; Schuman-Claeys, E.; Frija G. *Magn. Reson. Imaging* **1997**, 151025. (h) Berry, C.; Curtis, A. S. G. *J. Phys. D: Appl. Phys.* **2003**, *36*, R182.

(2) Grimm, S.; Schultz, M.; Barth, S.; Muller, R. *J. Mater. Sci.* **1997**, *32*, 1083.

(3) Stober, W.; Fink, A.; Bohn, E. *J. Colloid Interface. Sci.* **1968**, *26*, 62.

(4) Jean, J. H.; Ring, T. A. *Langmuir* **1986**, *2*, 251.

(5) Mounien, N.; Pileni, M. P. *Chem. Mater.* **1996**, *8*, 1128.

(6) Bonnemann, H.; Richards, R. M. *Eur. J. Inorg. Chem.* **2001**, 2455.

(7) Rosensweig, R. E. *Ferrohydrodynamics*; Cambridge University Press: Cambridge, U.K., 1985.

(8) Kim, D. K.; Zhang, Y.; Voit, W.; Rao, K. V.; Muhammed, M. *J. Magn. Mater.* 200, *225*, 30.

(9) Blum, A.; Cebers, A.; Maiorov, M. M. *Magnetic fluids*; de cruiter: Berlin, 1997.

(10) Shafi, K. V. P.M; Ulman, A.; Yan, X.; Yang, N. L.; Estourbes, C.; White H.; Rafalovich, M. *Langmuir* **2001**, *17*, 5093.

(11) Shafi, K. V. P. M.; Wizel, S.; Prozorov, T.; Gedanken A. *Thin Solid Films* **1998**, *318*, 38.

(12) Bacri, J.; Perzynski, R.; Salin, D.; Cabuil, V.; Massart, R. *J. Magn. Mater.* **1990**, *85*, 27.

(13) Khalafalla, S. E.; Reimers, G. W. *IEEE Trans. Magn. Mag.* **1980**, *16*, 178.

(14) Shen, L.; Stachowiak, A.; Seif-Eddeen, K. F.; Laibinis, P. E.; Hatton, *Langmuir* **2001**, *17*, 288.

(15) Shimoizaka, J.; Nakatsuka, K.; Fujita, T.; Kounosu, A. *IEEE Trans. Magn Mag.* **1980**, *16*, 368.

(16) Wormuth, K. *J. Colloid Interface Sci.* **2001**, *241*, 366.

(17) Pardoe, H.; Chau-Anusorn, W.; Pierre, T. G.; Dobson, J. *J. Magn. Magn. Mater.* **2001**, *225*, 41.

(18) Mendenhall, G. D.; Geng, Y.; Hwang, J. *J. Colloid Interface Sci.* **1996**, *184*, 519.

(19) Lee, J.; Isobe, T.; Senna, M. *J. Colloid Interface. Sci.* **1996**, *177*, 490.

(20) Palmacci, S.; Josephon, L; Groman, E. V. *Synthesis of Polymer Covered Superparamagnetic Oxide Colloids for Magnetic Resonance Contrast Agents or other Applications*; PCT WO 9505669, 1993, 8, 12.

(21) Ding, X. B.; Sun, Z. H.; Wan, G. X.; Jiang, Y. Y. *React. Funct. Polym.* **1998**, *38*, 11.

(22) Underhill, R. S.;Liu, G. *Chem. Mater.* **2000**, *12*, 2082.

(23) Abu Mukh-Qasem, R.; Gedanken, A. *J. Colloid Interface Sci.* **2005**, *284*, 489.

(24) Weller, D.; Moser, A. *IEEE Trans. Magn.* **1999**, *35*, 4423.

(25) Sun, S.; Murray, C. B.; Weller, D.; Folks, L.; Moser, A. *Science* **2000**, *287*, 1989.

(26) Lin, X. M.; Jaeger, H. M.; Sorensen, C. M.; Klabunde, K. J. *J. Phys. Chem. B* **2001**, *105*, 3353.

(27) Bartlett, P. N.; Birkin, P. R.; Ghanem, M. A. *Chem. Commun.* **2000**, 1671.

(28) Fink, J.; Kiely, Ch..; Bethell, D.; Schiffrin, D. J. *Chem. Mater.* **1998**, *10*, 922.

(29) Jensen, T. R.; Schatz, G. C.; Van Duyne, R. P. *J. Phys. Chem. B* **1999**, *103*, 2394.

(30) Petit, C.; Taleb, A.; Pieleni, M. P. *J. Phys. Chem. B* **1999**, *103*, 1805.

(31) Wang, Z. L. *Adv. Mater.* **1998**, *10*, 10.

(32) Hulteen, J. C.; Treichel, D. A.; Smith, M. T.; Duval, M. L.; Jensen, T. R.; Van-Duyne, R. P. *J. Phys. Chem. B* **1999**, *103*, 3854.

(33) Michael, H.; Bernd, T.; Michael, G. *Aust. J. Chem* **2001**, *54*, 497.

(34) Jung, C. W. *Mag. Reson. Imaging* **1995**, *13*, 675.

(35) Leslie-Pelecky, D. L.; Rieke, R. D. *Chem. Mater.* **1996**, *8*, 1770.

(36) Lee, L. T.; Somasundaran. *Langmuir* **1989**, *5*, 854.

(37) Vijayakumar, R.; Koltypin, Y.; Felner, I.; Gedanken, A. *Mater. Sci. Eng.* **2000**, *A286*, 101.

(38) Feigel, F. *Spot Tests, Inorganic Applications*; Elsevier: New York, 1954; Vol. 1, pp 154−155.

(39) Kessler, D. A.; Koplik, J.; Levine, H. *Adv. Phys.* **1988**, *37*, 255.

(40) Pieters, R.; Langer, J. S. *Phys. Rev. Lett.* **1986**, *56*, 1948.

(41) Witten, T. A.; Sander, L. M. *Phys. Rev. B* **1983**, *27*, 5696

(42) Jeffrey, W.; Gilman; David, L.; VanderHart; Takashi Kashiwagi. *Fire and polymers II: Materials and Test for hazard prevention*; American Chemical Society: Washington, D.C.,1994; Chapter 11, p 161.

(43) Cornell, R. M.; Schwertmann, U. *The Iron Oxides: Structure, Properties Reactions, Occurrence, and Uses*; Wiley-VCH: Weinheim, 2003; p 28.

(44) Fried et al. *Adv. Mater.* **2001**.

(45) Sahoo et al. *J. Phys. Chem. B* **2005**.

(46) Wiedwald et al. *J. Vac. Sci. Technol.* **2001**.

(47) Michael, H.; Bernd, T.; Giersig, M. *Aust. J. Chem.* **2001**, *54*, 497.

(48) Spasova, M.; Wiedwald, U.; Ramchal, R.; Farle, M.; Hilgendorff, M.; Giersig, M.; *J. Magn. Magn. Mater.* **2002**, *240*, 40.

(49) Gedanken, A. *Curr. Science* **2003**, *85*, 12.

(50) Klug, H., Alexander, L., Eds.; *X-ray Diffraction Procedures*; Wiley: New York, 1962; p 125.

(51) Wizel, S.; Margel, S.; Gedanken, A. *J. Mater. Res.* **1999**, *14*, 10.

(52) Wizel, S.; Prozorov, R.; Cohen,Y.; Aurbach, D.; Margel, S.; Gedanken, A. *J. Mater. Res.* **1998**, *13*, 1.